Electronic Supplementary Information (ESI)

Ultralow-content Pt nanodots/Ni₃Fe nanoparticles: interlayer nanoconfinement synthesis and overall water splitting

Yajun Ni,[a,‡] Wei Zhang,[a,c,‡] Yaru Li,[a] Shui Hu,[b,*] Hong Yan,[a,*] and Sailong Xu[a,c,*]

[a]State Key Laboratory of Chemical Resource Engineering, [b]State Key Laboratory of Organic-Inorganic Composites, Beijing University of Chemical Technology, Beijing 100029, China. E-mail: xusl@mail.buct.edu.cn (S.X.); yanhong@mail.buct.edu.cn (H.Y.); hushui@mail.buct.edu.cn

[c]Quzhou Institute for Innovation in Resource Chemical Engineering, Quzhou 324003, China

‡These authors contributed equally to this work.

Experimental Section

Theoretical calculations

For Ni₃Fe, γ-NiOOH, the real active species of the oxygen evolution reaction catalyst, is used as a prototype, and K$^+$ and protons are cross-solvated because 1 M KOH is used as the electrolyte in the experiments.[1-4] The cell parameters are α = 90°, β = 90°, γ = 90°, a = 8.523 Å, b = 9.991 Å, and c = 15.469 Å. For Pt/Ni₃Fe, the (100) crystallographic plane of 4 × 3 × 1 is chosen for doping Pt nanodots. Because (100) is a high index crystal plane, this plane exposes unsaturated metal sites, which facilitates the adsorption and desorption of oxygenated intermediates at the metal sites. The chemical formula of Ni₃Fe is $(Fe)_3K_4(Ni)_9H_{17}O_{32}$, and the chemical formula of Pt/Ni₃Fe is $(Fe)_3PtK_4(Ni)_8H_{17}O_{32}$.

For Pt, the Pt(111) is employed with the lattice parameters of a = 8.32 Å, b = 8.32 Å, c = 24.53 Å. A 15 Å vacuum layer is built up in the c-axis to avoid modeling in the periodicity in the c-axis direction.
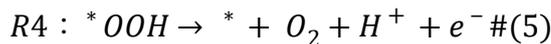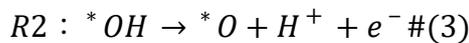
Computational Methods

Density Functional Theory is calculated using Materials studio software 6.1 (Accelrys Software Inc., San Diego, CA). The calculations in this paper were all carried out using the CASTEP module.[5,6] The Perdew-Burke-Ernzerhof (PBE) exchange

correlation in the generalized gradient approximation (GGA)[7] was used in the calculations. However, transition metal systems containing d electrons have strong electron-electron interactions that cannot be accurately described by DFT methods. Hubbard-corrected density functional theory was used. The electronic density of states of the hydroxyl oxides were calculated by setting the Ueff values for Ni, and Fe to 6.45,[8] and 4.30 eV,[9] respectively. The energy and displacement convergence standards are 5×10^{-5} eV and 0.005 Å, respectively. The k-point grid in the Brillouin zone is set to be $3 \times 3 \times 1$ by the Monkhorst-Pack scheme. The cut-off energy is 420 eV.

When the pH is fixed at 0, the entire OER[10] can be defined as

$$2H_2O \rightarrow O_2 + 4H^+ + 4e^- \quad \#(1)$$

The following are the four electronic reaction steps of the OER approach: In the first step, the catalyst (denoted as *) absorbs an H_2O molecule from the solvent and releases $H^+ + e^-$, leading to the formation of *OH. Next, the $H^+ + e^-$ pair continues to separate from *OH, leaving *O. Then, another H_2O molecule joins and reacts with *O to form *OOH, while releasing $H^+ + e^-$. Finally, *OOH can form O_2 and return to *, while releasing a $H^+ + e^-$ pair.

$$R1 : H_2O + {}^* \rightarrow {}^*OH + H^+ + e^- \quad \#(2)$$

$$R2 : {}^*OH \rightarrow {}^*O + H^+ + e^- \quad \#(3)$$

$$R3 : {}^*O + H_2O \rightarrow {}^*OOH + H^+ + e^- \quad \#(4)$$

$$R4 : {}^*OOH \rightarrow {}^* + O_2 + H^+ + e^- \quad \#(5)$$

In the calculation of the OER overpotential, the standard hydrogen electrode approximation is used, and the standard hydrogen electrode is an assumed ideal state in which $\frac{1}{2} H_2 \rightarrow H^+ + e^-$.[11] The Energy, entropic contribution and zero point energies[12] of hydrogen, oxygen, and water molecules are listed in Table S1.

The Gibbs free energy difference for all of the above primitive steps (ΔG_{*OH}, ΔG_{*O}, ΔG_{*OOH}) contains an electron transfer calculated by Eq. (6):

$$\Delta G = \Delta E + \Delta ZPE - T\Delta S + \Delta G_U + \Delta G_{pH} \# (6)$$

In this equation ΔE, ΔZPE and ΔS represent the difference in adsorption energy, zero point energy, and entropy, respectively. The adsorption energy ΔE (E_{ads}) was calculated using DFT. The values of ΔZPE and ΔS were calculated using standard thermodynamic data and density functional theory. $\Delta G_U = -eU$, where U represents the potential based

on a standard hydrogen electrode. ΔG_{pH} represents the Gibbs free energy correction with respect to pH, which can be calculated by $\Delta G_{pH} = -K_B T \ln 10 \cdot pH$, with K_B being the Boltzmann constant (1.380649×10^{-23} J K^{-1}), where the temperature is 298.15 K. The sum of ΔG_1, ΔG_2, ΔG_3 and ΔG_4 is equal to the Gibbs free-energy change for the total reaction $2H_2O(l) \rightarrow 2H_2\,(g)\, + O_2(g)$, i.e., 4.92 eV. Since, in the calculation of the Gibbs function, the standard hydrogen electrode assumption, and in that assumption pH = 0 and U = 0, both ΔG_U and ΔG_{pH} are 0 in Eqs. 6. The value of the OER overpotential (η^{OER}) is unaffected by either the electrolyte pH or the applied bias voltage (U).

The change in Gibbs free energy during OER is defined as

$$\Delta G_1 = \Delta G_{*OH} \#(7)$$

$$\Delta G_2 = \Delta G_{*O} - \Delta G_{*OH} \#(8)$$

$$\Delta G_3 = \Delta G_{*OOH} - \Delta G_{*O} \#(9)$$

$$\Delta G_4 = 4.92 - \Delta G_{*OOH} \#(10)$$

A theoretical system is constructed to systematically evaluate the performance of different catalysts for oxygen evolution reaction in alkaline electrolytes. The free energies of the four-electron transfer radical steps of the ideal OER catalysts at zero potential should be equal, i.e., 4.92 V / 4 = 1.23 V vs. the standard reversible hydrogen electrode (RHE), in other words, the Gibbs free energies of all the four-electron transfer reactions at a starting potential of 1.23 V are 0 eV, and the exceeding value is defined as an overpotential if the actual potential is greater than 1.23 V. The overpotential η_{OER} is given by Eq. (11):

$$\eta^{OER} = \left(\frac{\Delta G^{OER}}{e}\right) - 1.23\ V, \Delta G^{OER} = \max\left[\Delta G_1, \Delta G_2, \Delta G_3, \Delta G_4\right] \#(11)$$

The Gibbs free energy calculation for hydrogen evolution reaction can be calculated by Eq. (12):

$$\Delta G_{*H} = \Delta E_{*H} + \Delta ZPE - T\Delta S \#(12)$$

In which ΔG_{*H} is the adsorption energy of hydrogen atom on the crystal surface, ΔZPE is the zero point energy difference between adsorbed hydrogen and hydrogen in the gas phase, and ΔS is the entropy change of *H adsorption.

References

1. J. Zaffran, M. B. Stevens, C. D. M. Trang, M. Nagli, M. Shehadeh, S. W. Boettcher and M. Caspary Toroker, *Chem. Mater.*, 2017, **29**, 4761-4767.

2. H. Shin, H. Xiao and W. A. Goddard, *J. Am. Chem. Soc.*, 2018, **140**, 6745-6748.

3. J. G. Baker, J. R. Schneider, J. A. Garrido Torres, J. A. Singh, A. J. M. Mackus, M. Bajdich and S. F. Bent, *ACS Appl. Energy Mater.*, 2019, **2**, 3488-3499.

4. X. Zheng, J. Tang, A. Gallo, J. A. Garrido Torres, X. Yu, C. J. Athanitis, E. M. Been, P. Ercius, H. Mao, S. C. Fakra, C. Song, R. C. Davis, J. A. Reimer, J. Vinson, M. Bajdich and Y. Cui, *PNAS*, 2021, **118**, e2101817118.

5. M. D. Segall, J. D. L. Philip, M. J. Probert, C. J. Pickard, P. J. Hasnip, S. J. Clark and M. C. Payne, *Condens. Matter*, 2002, **14**, 2717.

6. M. C. Payne, M. P. Teter, D. C. Allan, T. A. Arias and J. D. Joannopoulos, *Rev. Mod. Phys.*, 1992, **64**, 1045-1097.

7. J. P. Perdew, K. Burke and M. Ernzerhof, *Phys. Rev. Lett.*, 1996, **77**, 3865.

8. A. Jain, G. Hautier, S. P. Ong, C. J. Moore, C. C. Fischer, K. A. Persson and G. Ceder, *Phys. Rev. B*, 2011, **84**, 045115.

9. J. M. P. Martirez and E. A. Carter, *J. Am. Chem. Soc.*, 2018, **141**, 693-705.

10. E. Skúlason, T. Bligaard, S. Gudmundsdóttir, F. Studt, J. Rossmeisl, F. Abild-Pedersen, T. Vegge, H. Jónsson and J. K. Nørskov, *Phys. Chem. Chem. Phys.*, 2012, **14**, 1235-1245.

11. J. K. Nørskov, J. Rossmeisl, A. Logadottir, L. Lindqvist, J. R. Kitchin, T. Bligaard and H. Jónsson, *J. Phys. Chem. B*, 2004, **108**, 17886.

12. P. Liao, J. A. Keith and E. A. Carter, *J. Am. Chem. Soc.*, 2012, **134**, 13296-13309.
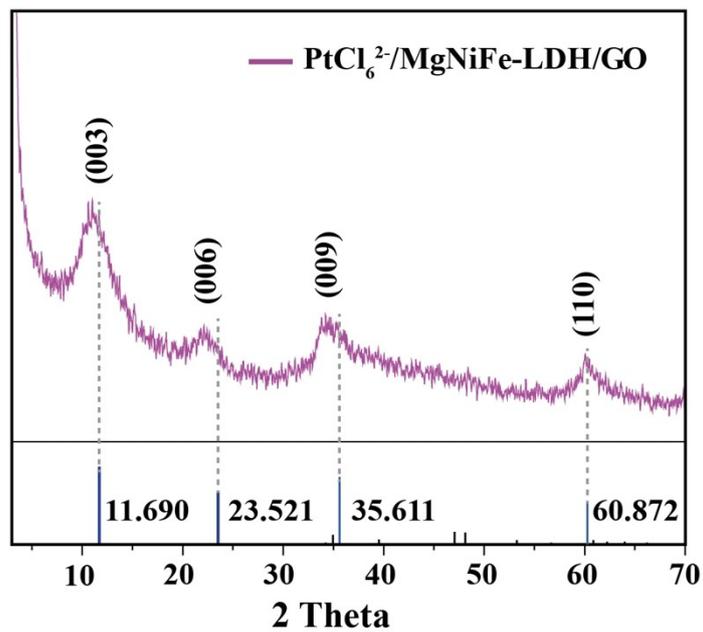
Figure S1

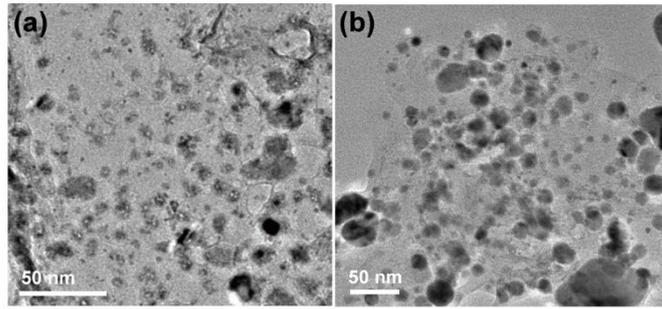**Figure S1** The XRD pattern of the $PtCl_6^{2-}$/MgNiFe-LDH/GO precursor.

Figure S2 TEM images of (a) Pt/Ni$_3$Fe/rGO after etching MgO, and (b) Pt/Ni$_3$Fe/rGO that was directly derived from a Mg-free PtCl$_6^{2-}$/NiFe-LDH precursor.
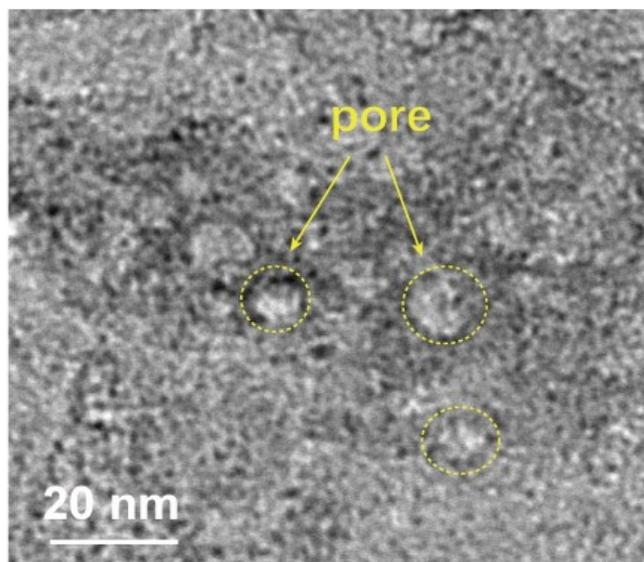
Figure S3

Figure S3 The HRTEM image shows the presence of pores of the Pt/Ni₃Fe/rGO catalyst after selectively removing the MgO that was formed from the MgNiFe-LDH during the calcination.
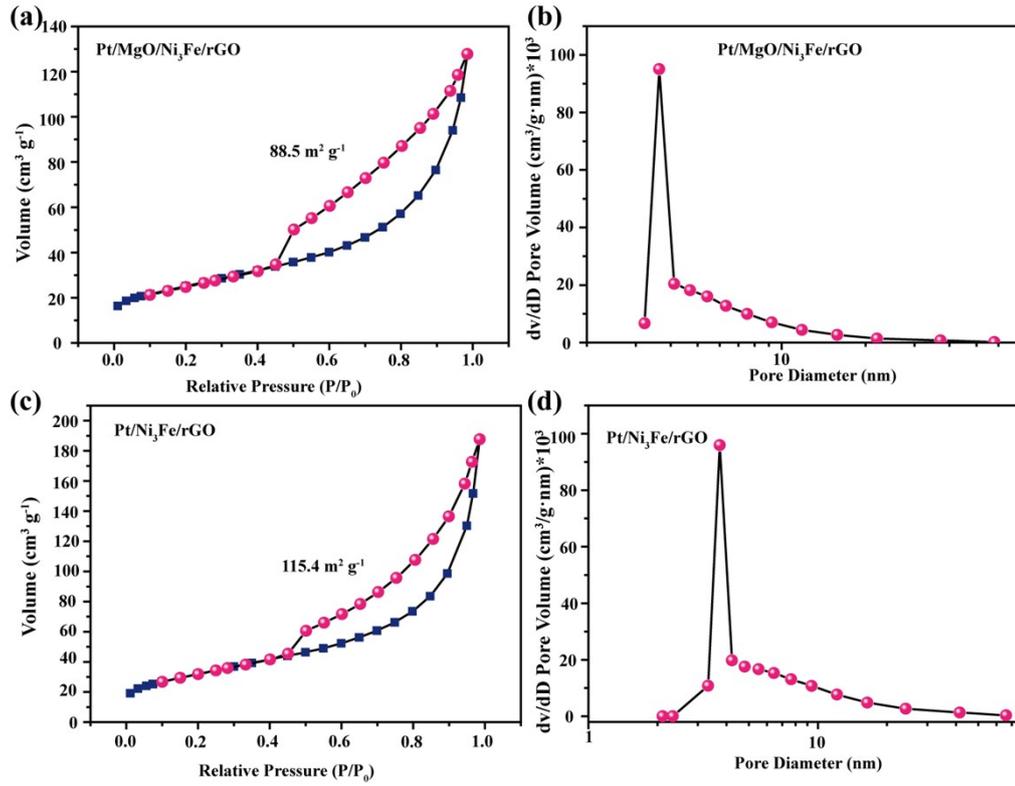
Figure S4

Figure S4 (a) N_2 adsorption and desorption isotherms and (b) the pore size distribution of the Pt/MgO/Ni$_3$Fe/rGO intermediate composite, (c) N_2 adsorption and desorption isotherms and (d) the pore size distribution of the Pt/Ni$_3$Fe/rGO composite after the selective removal of MgO.
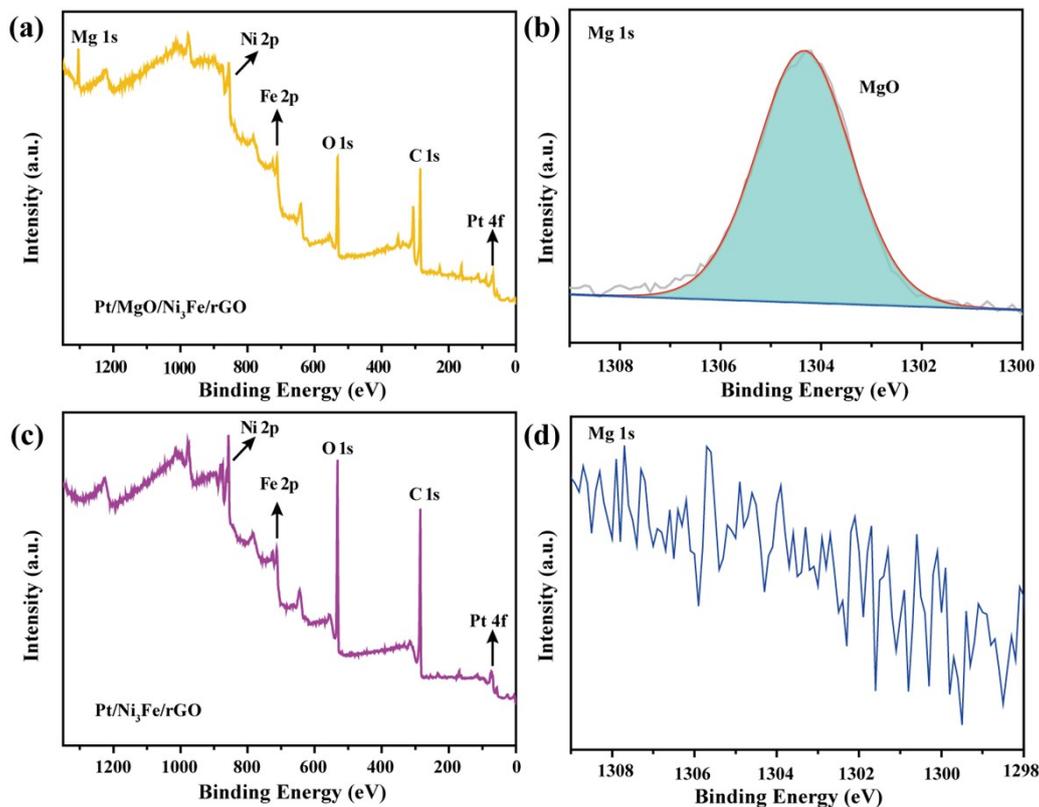
Figure S5 Comparison of XPS spectra: (a) a full scan survey and (b) Mg1s spectra for the Pt/MgO/Ni$_3$Fe/rGO intermediate composite; (c) a full scan survey and (d) Mg 1s spectra for the Pt/Ni$_3$Fe/rGO composite, showing no signal of Mg 1s.
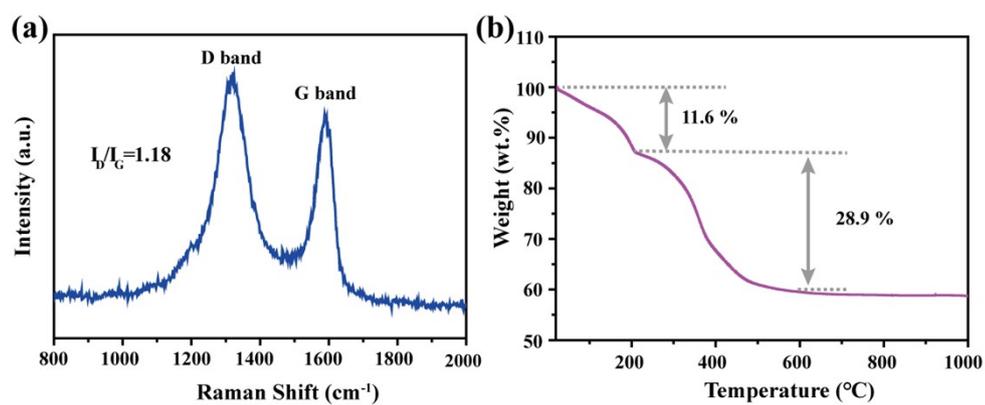
Figure S6

Figure S6 (a) Raman spectrum and (b) TG analysis of the Pt/Ni$_3$Fe/rGO composite.

Figure S7
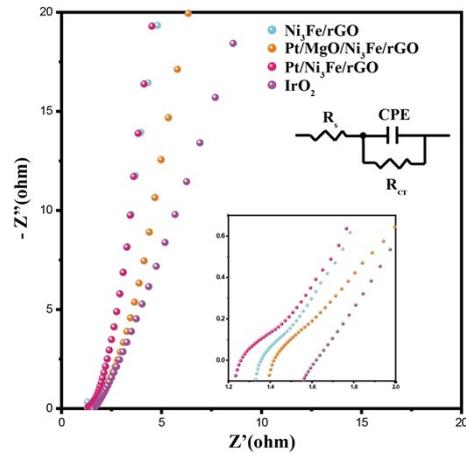
Figure S7 Electrochemical impedance spectra of Pt/Ni₃Fe/rGO, Pt/MgO/Ni₃Fe/rGO, Ni₃Fe/rGO, IrO₂ for the OER.
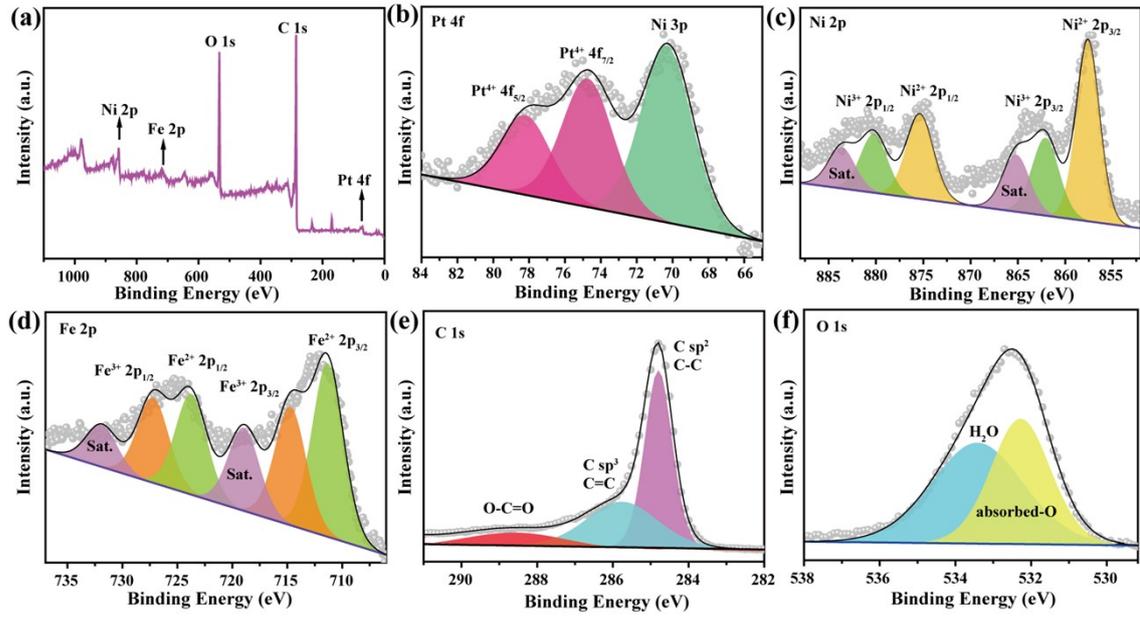
Figure S8 XPS spectra of the Pt/Ni$_3$Fe/rGO composite after OER stability test: (a) a full scan survey, (b) Pt 4f, (c) Ni 2p, (d) Fe 2p, (e) C 1s and (f) O 1s.

Figure S9
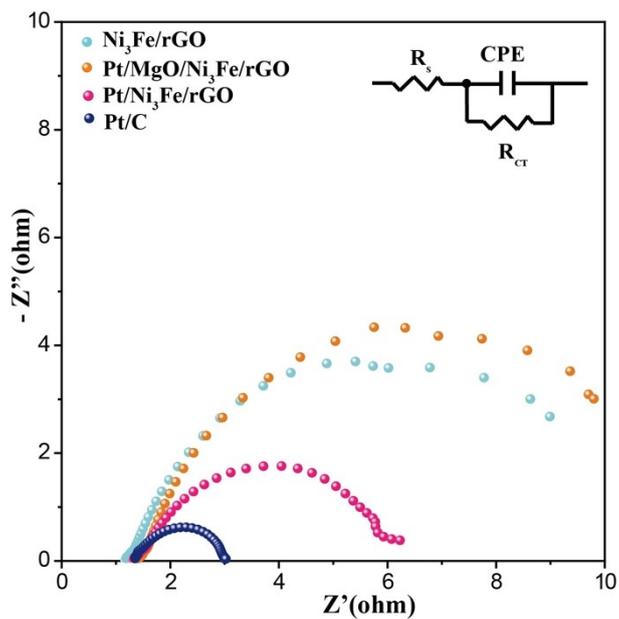
Figure S9 Electrochemical impedance spectra of Pt/Ni₃Fe/rGO, Pt/MgO/Ni₃Fe/rGO, Ni₃Fe/rGO, Pt/C for the HER.

Figure S10
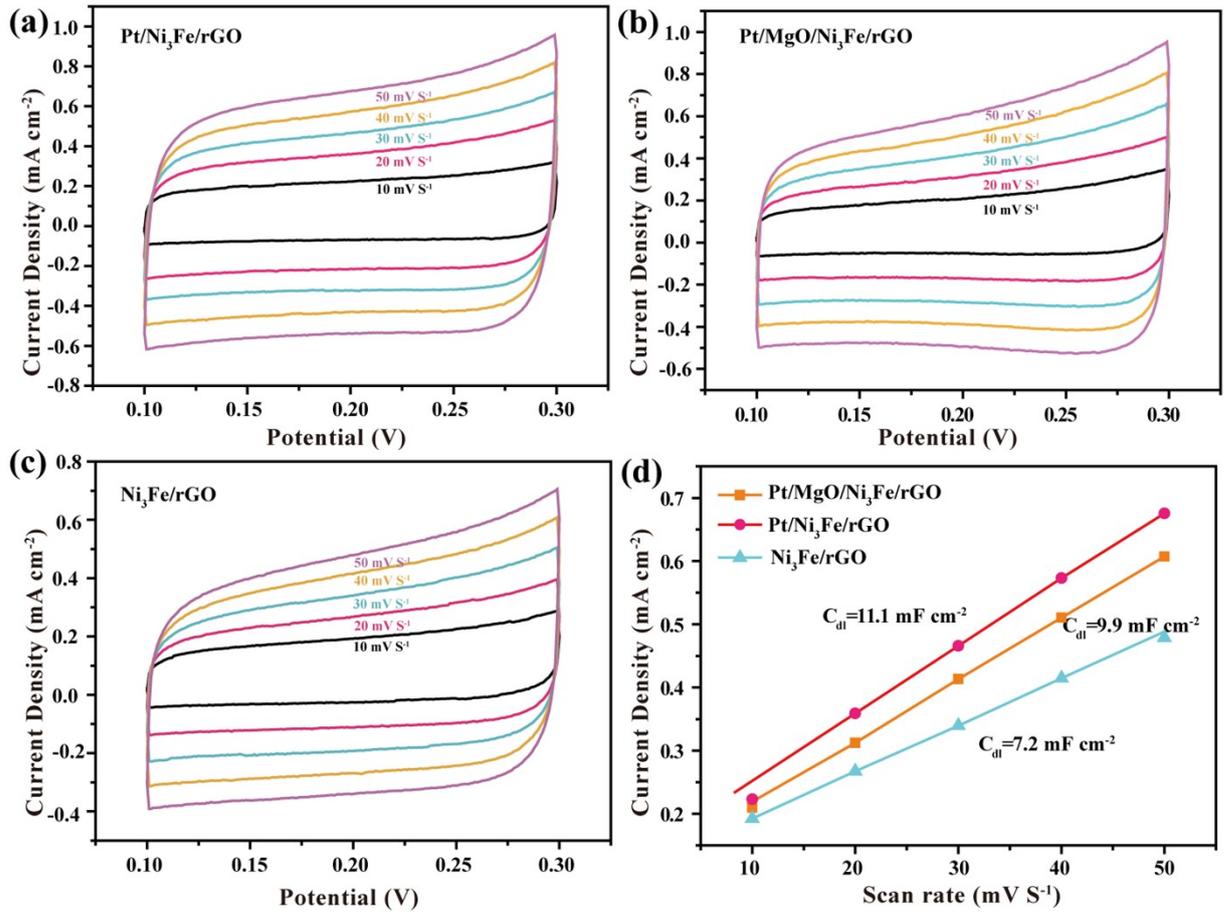
Figure S10 Cyclic voltammograms (CVs) for (a) Pt/Ni$_3$Fe/rGO, (b) Pt/MgO/Ni$_3$Fe/rGO, (c) Ni$_3$Fe/rGO measured at different scan rates from 10 to 50 mV/s and (d) corresponding C$_{dl}$ at 0.2 V vs Ag/AgCl.

Figure S11
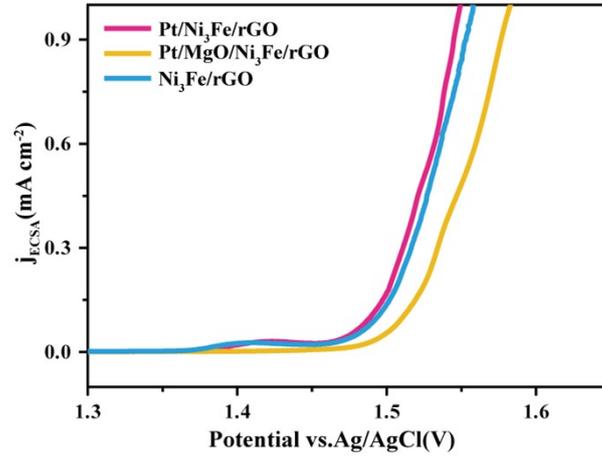
Figure S11 LSV curves of OER normalized by ECSA of Pt/Ni$_3$Fe/rGO, Pt/MgO /Ni$_3$Fe/rGO, and Ni$_3$Fe/rGO.
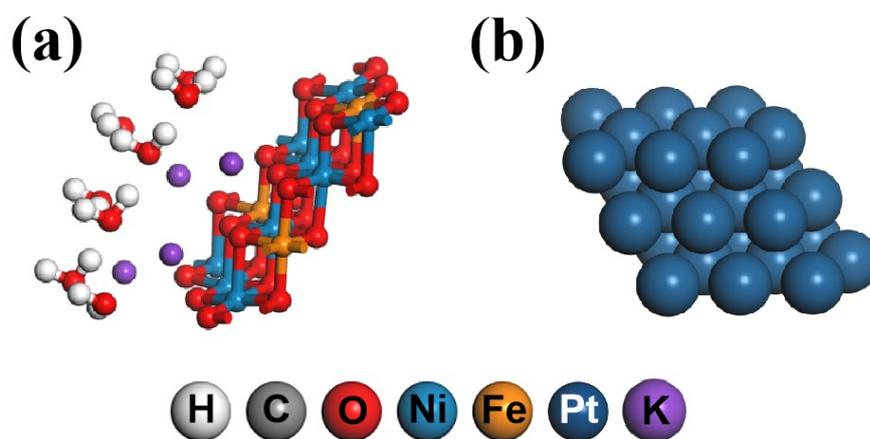
Figure S12 Optimized structures of (a) Ni$_3$Fe and (b) Pt(111).

Table S1

Energy, entropic contribution, zero point energy, and Gibbs free energy of H_2, O_2, and H_2O.

Molecular	Energy（eV）	Entropic（eV）	Zero point energy（eV）	Gibbs free energy
H_2(g)	-30.87	0.40	0.27	-31.00
O_2(g)	-868.41	0.63	0.10	-868.94
H_2O(l)	-467.83	0.67	0.57	-467.93

Table S2

ICP analysis for Ni, Fe, Pt of Pt/Ni$_3$Fe/rGO composite.

Element	Ni	Fe	Pt
Content /wt%	33.15	10. 42	0.71

Table S3

R_{ct} values of Pt/Ni$_3$Fe/rGO, Pt/MgO/Ni$_3$Fe/rGO, Ni$_3$Fe/rGO and IrO$_2$ for the OER.

Catalyst	Pt/Ni$_3$Fe/rGO	Pt/MgO/Ni$_3$Fe/rGO	Ni$_3$Fe/rGO	IrO$_2$
R_{ct}/Ω	1.3	4.1	2.2	9.3

Table S4

R_{ct} values of Pt/Ni$_3$Fe/rGO, Pt/MgO/Ni$_3$Fe/rGO, Ni$_3$Fe/rGO and IrO$_2$ for the HER.

Catalyst	Pt/Ni$_3$Fe/rGO	Pt/MgO/Ni$_3$Fe/rGO	Ni$_3$Fe/rGO	Pt/C
R_{ct}/Ω	3.2	6.7	5.6	1.4

Table S5

Comparison of the OER performance between the Pt/Ni$_3$Fe/rGO composite and those Pt-based electrocatalysts reported previously (in 1.0 M KOH).

Catalysts	Pt content (wt%)	Overpotential (mV)	Tafel (mv dec^{-1})	References
Pt-NiO/Gr-SUS	0.09	240	101.2	1
Pt-SnFeNi/CF	0.42	-	103	2
NF-Na-Fe-Pt	0.60	261	39.68	3
Pt–αFe$_2$O$_3$/NF	2.05	304	49.6	4
Pt-WO$_3$-x@rGO	1.58	174	48	5
Pt$_1$@Fe-N-C	2.10	310	62	6
Pt-Ni$_3$Se$_2$@NiOOH/NF	8.20	-	31	7
Pt/NiFeV	16.80	-	48	8
Pt/LiCoO$_2$	30.00	258	46.8	9
PtIr/IrOx-50	50.97	266	44	10
Pt-NiFe PBA	-	210	43.5	11
NM@Pt$_{0.15}$-Ni(OH)$_2$	-	309	52	12
B-Pt-NiFe-LDH	0.781	208	30.4	13
Pt/Ni$_3$Fe/rGO	0.71	240	35	**This work**

Table S6

Comparison of the HER performance between the Pt/Ni$_3$Fe/rGO composite and those Pt-based electrocatalysts reported previously (in 1.0 M KOH).

Catalysts	Pt content (wt%)	Overpotential (mV)	Tafel (mv dec^{-1})	References
Pt-NiO/Gr-SUS	0.09	79	41	1
Pt-SnFeNi/CF	0.42	20	-	2
NF-Na-Fe-Pt	0.60	31	35.98	3
Pt–αFe$_2$O$_3$/NF	2.05	90	50.6	4
Pt-WO$_3$-x@rGO	1.58	37	35	5
Pt$_1$@Fe-N-C	2.10	60	42	6
Pt-Ni$_3$Se$_2$@NiOOH/NF	8.20	46	45	7
Pt/NiFeV	16.80	19	33	8
Pt/LiCoO$_2$	30.00	61	39.5	9
PtIr/IrOx-30	69.80	20	38	10
Pt-NiFe PBA	-	29	58.3	11
Pt/SnS$_2$	0.37	117	69	14
hcp Pt-Ni	30.16	65	78	15
Pt-Ni/LDH	5.50	52	47	16
Pt1/Co(OH)$_2$/C	1.41	50	48.7	17
Pt/Ni$_3$Fe/rGO	0.71	76	43	**This work**

Table S7

Comparison of overall-water-splitting performance at 10 mA cm^{-2} between the Pt/Ni$_3$Fe/rGO composite and those Pt-based electrocatalysts reported previously (in 1.0 M KOH).

Catalysts	Pt content (wt%)	Overall voltage (V)	Durability (h)	References
Pt-NiO/Gr-SUS	0.09	1.6	12	1
NF-Na-Fe-Pt	0.60	1.56	12	3
Pt-αFe$_2$O$_3$/NF	2.05	1.51	50	4
Pt-WO$_{3-x}$@rGO	1.58	1.55	12	5
Pt-Ni$_3$Se$_2$@NiOOH/NF	8.20	1.52	12	7
Pt-NiMoO$_4$-GO/NF	4.63	1.515	48	18
Pt-CoS$_2$/CC	4.5	1.55	20	19
Pt-Cu@CuxO NWs/3DF	0.74	1.56	27	20
Pt-Ni$_{2/3}$Fe$_{1/3}$(OH)$_2$	6.15	-	15	21
PtCo-FeCo PBAs	8.4	1.68	50	22
Pt/VC	2.84	1.59	12	23
Pt/Ni$_3$Fe/rGO	0.71	1.55	50	**This work**

References

1. S. Jeong, H. D. Mai, K.-H. Nam, C.-M. Park and K.-J. Jeon, *ACS Nano*, 2022, **16**, 930-938.

2. S. Li, R. Ma, Y. Lu, Y. Pei, M. Yang, J. Wang and D. Liu, *J. Mater. Chem. A*, 2020, **8**, 5919-5926.

3. Y. Zhao, Y. Gao, Z. Chen, Z. Li, T. Ma, Z. Wu and L. Wang, *Appl. Catal. B*, 2021, **297**, 120395.

4. B. Ye, L. Huang, Y. Hou, R. Jiang, L. Sun, Z. Yu, B. Zhang, Y. Huang and Y.

Zhang, *J. Mater. Chem. A*, 2019, **7**, 11379-11386.

5. D. Yin, Y.-D. Cao, D.-F. Chai, L.-L. Fan, G.-G. Gao, M.-L. Wang, H. Liu and Z. Kang, *Chem. Eng. J,* 2022, **431**, 133287.

6. X. Zeng, J. Shui, X. Liu, Q. Liu, Y. Li, J. Shang, L. Zheng and R. Yu, *Adv. Energy Mater.*, 2017, **8**, 1701345.

7. X. Zheng, Y. Cao, X. Han, H. Liu, J. Wang, Z. Zhang, X. Wu, C. Zhong, W. Hu and Y. Deng, *Sci. China Mater.,* 2019, **62**, 1096-1104.

8. Y. Feng, Z. Li, S. Li, M. Yang, R. Ma and J. Wang, *J. Energy Chem.*, 2022, **66**, 493-501.

9. X. Zheng, P. Cui, Y. Qian, G. Zhao, X. Zheng, X. Xu, Z. Cheng, Y. Liu, S. X. Dou and W. Sun, *Angew. Chem. Int. Ed.*, 2020, **59**, 14533-14540.

10. H. Huang, L. Fu, W. Kong, H. Ma, X. Zhang, J. Cai, S. Wang, Z. Xie and S. Xie, *Small*, 2022, **18**, 2201333.

11. Z. Chen, D. Liu, Y. Gao, Y. Zhao, W. Xiao, G. Xu, T. Ma, Z. Wu and L. Wang, *Sci. China Mater.*, 2021, **65**, 1217-1224.

12. J. Zhang, M. Yang, X. Zhu, J. Dang, J. Ma, B. Liu, T. Huang, M. Ouyang and F. Yang, *Chem. Eng. J.*, 2023, **476**, 146576.

13. L. Tan, H. Wang, C. Qi, X. Peng, X. Pan, X. Wu, Z. Wang, L. Ye, Q. Xiao, W. Luo, H. Gao, W. Hou, X. Li and T. Zhan, *Appl. Catal. B*, 2024, **342**, 123352.

14. F. Xia and F. Yang, *Energy Fuels*, 2022, **36**, 4992-4998.

15. Z. Cao, Q. Chen, J. Zhang, H. Li, Y. Jiang, S. Shen, G. Fu, B.-a. Lu, Z. Xie and L. Zheng, *Nat. Commun.*, 2017, **8**, 15131.

16. W. Yi, R. Yu, H. Jiang, J. Wu and G. J. Cheng, *Adv. Funct. Mater.*, 2024, **34**, 2308575.

17. A. Pei, R. Xie, Y. Zhang, Y. Feng, W. Wang, S. Zhang, Z. Huang, L. Zhu, G. Chai, Z. Yang, Q. Gao, H. Ye, C. Shang, B. H. Chen and Z. Guo, *Energy Environ. Sci.*, 2023, **16**, 1035-1048.

18. J. Zhang, S. Zhang, X. Zhang, Z. Ma, Z. Wang and B. Zhao, *J. Colloid Interf. Sci.*, 2023, **650**, 1490-1499.

19. X. Han, X. Wu, Y. Deng, J. Liu, J. Lu, C. Zhong and W. Hu, *Adv. Energy Mater.*, 2018, **8**, 1800935.

20. D. T. Tran, H. T. Le, T. L. Luyen Doan, N. H. Kim and J. H. Lee, *Nano Energy*, 2019, **59**, 216.

21. L. Wang, L. Zhang, W. Ma, H. Wan, X. Zhang, X. Zhang, S. Jiang, J. Y. Zheng and Z. Zhou, *Adv. Funct. Mater.*, 2022, **32**, 2203342.

22. C. Zeng, Q. Li, Y. You, L. Sun, W. Cheng, X. Zheng, S. Liu and Q. Wang, *Int. J. Hydrogen Energy*, 2022, **47**, 35149.

23. N. Wang, X. Bo and M. Zhou, *ACS Appl. Mater. Interfaces*, 2022, **14**, 23332-23341.